Article

Structure

# Short Linear Sequence Motif LxxPTPh Targets Diverse Proteins to Growing Microtubule Ends

## Highlights

- The LxxPTPh motif interacts with the C-terminal domain of EB
- The EB-LxxPTPh interaction does not require the C-terminal tail of EB
- LxxPTPh motifs target diverse proteins to growing microtubule ends
- The knowledge of LxxPTPh motifs provides a basis to discover and study novel +TIPs

## Authors

Anil Kumar, Cristina Manatschal, Ankit Rai, ..., Richard A. Kammerer, Anna Akhmanova, Michel O. Steinmetz

## Correspondence

michel.steinmetz@psi.ch

## In Brief

Kumar et al. show that the LxxPTPh motif targets diverse +TIPs to growing microtubule ends in an end-binding (EB)-dependent manner. The interaction of LxxPTPh with EB does not depend on the C-terminal tail of EB. The results provide a basis to discover and study novel +TIPs.

Kumar et al., 2017, Structure *25*, 924–932
June 6, 2017 
http://dx.doi.org/10.1016/j.str.2017.04.010

CellPress

Structure
Article

# Short Linear Sequence Motif LxxPTPh Targets Diverse Proteins to Growing Microtubule Ends

Anil Kumar,[1] Cristina Manatschal,[1,4] Ankit Rai,[2] Ilya Grigoriev,[2] Miriam Steiner Degen,[1] Rolf Jaussi,[1] Ines Kretzschmar,[3] Andrea E. Prota,[1] Rudolf Volkmer,[3] Richard A. Kammerer,[1] Anna Akhmanova,[2] and Michel O. Steinmetz[1,5,*]

[1]Laboratory of Biomolecular Research, Division of Biology and Chemistry, Paul Scherrer Institut, 5232 Villigen PSI, Switzerland
[2]Cell Biology, Faculty of Science, Utrecht University, 3584 CH Utrecht, the Netherlands
[3]Institut für Medizinische Immunologie, Charité-Universitätsmedizin Berlin, Leibniz-Institut für Molekulare Pharmakologie, 10117 Berlin, Germany
[4]Present address: Department of Biochemistry, University of Zürich, 8057 Zürich, Switzerland
[5]Lead Contact
*Correspondence: michel.steinmetz@psi.ch
http://dx.doi.org/10.1016/j.str.2017.04.010

## SUMMARY

**Microtubule plus-end tracking proteins (+TIPs) are involved in virtually all microtubule-based processes. End-binding (EB) proteins are considered master regulators of +TIP interaction networks, since they autonomously track growing microtubule ends and recruit a plethora of proteins to this location. Two major EB-interacting elements have been described: CAP-Gly domains and linear SxIP sequence motifs. Here, we identified LxxPTPh as a third EB-binding motif that enables major +TIPs to interact with EBs at microtubule ends. In contrast to EB-SxIP and EB-CAP-Gly, the EB-LxxPTPh binding mode does not depend on the C-terminal tail region of EB. Our study reveals that +TIPs developed additional strategies besides CAP-Gly and SxIP to target EBs at growing microtubule ends. They further provide a unique basis to discover novel +TIPs, and to dissect the role of key interaction nodes and their differential regulation for hierarchical +TIP network organization and function in eukaryotic organisms.**

## INTRODUCTION

Microtubule plus-end tracking proteins (+TIPs) are a large, evolutionary conserved group of diverse microtubule-associated proteins, which specifically bind the growing ends of microtubules. As such, +TIPs play important roles in virtually all microtubule-based processes, including cell division, motility, and intracellular trafficking (reviewed in Akhmanova and Steinmetz, 2015). A key property of most +TIPs is their ability to form interaction networks that regulate microtubule dynamics or attachment of microtubule plus ends to subcellular structures such as actin bundles, kinetochores, the ER, or the cell cortex (reviewed in Akhmanova and Steinmetz, 2015). Defining the exact interaction modes within +TIP networks is a prerequisite to understand and interfere with +TIP network function, and is the focus of intense ongoing research.

The members of the highly conserved end-binding protein (EB) family are +TIPs that autonomously recognize and track the growing ends of microtubules. EBs contain an N-terminal calponin homology domain that specifically recognizes and binds microtubule tips, and a C-terminal dimerization domain that interacts with +TIP partners (reviewed in Akhmanova and Steinmetz, 2015; Galjart, 2010; Slep, 2010; Kumar and Wittmann, 2012). The C-terminal domain contains a parallel two-stranded coiled-coil motif, an EB homology (EBH) domain, and a disordered C-terminal tail region (Honnappa et al., 2005, 2009; Slep et al., 2005). Owing to their unique biochemical activities, i.e., autonomous microtubule-tip tracking and recruitment of +TIP partners, EBs are generally acknowledged to represent master regulators of +TIP networks (reviewed in Akhmanova and Steinmetz, 2015; Galjart, 2010; Slep, 2010; Kumar and Wittmann, 2012). Assessing the mechanisms by which +TIPs interact with EBs is thus key to understanding how important cytoskeletal regulators interact with growing microtubule ends to control their cellular functions.

Only two EB-interacting +TIP elements have been described until now: globular CAP-Gly (cytoskeleton-associated protein glycine-rich) domains and short linear SxIP sequence motifs (where x represents any amino acid) that occur in disordered and basic sequence regions of +TIPs. However, recent findings suggest that additional unknown +TIP elements besides CAP-Gly domains or SxIP motifs must exist, which organize +TIP networks. Kar9, for example, is a +TIP that mediates the interaction of growing microtubule plus ends with actin cables to enable nuclear movements during mating (Kurihara et al., 1994; Molk et al., 2006) and correct spindle positioning during metaphase in budding yeast (Liakopoulos et al., 2003; Miller and Rose, 1998; Korinek et al., 2000). Kar9 contains one SxIP-like- and one canonical SxIP motif in its C terminus, which binds the C-terminal domain of the budding yeast EB ortholog Bim1 (Manatschal et al., 2016) (Figure 1A). However, mutating both the motifs did not abrogate binding to Bim1 and tracking of growing microtubule ends of Kar9 (Manatschal et al., 2016). Collectively, these studies strongly suggest that additional unknown elements must exist besides CAP-Gly and SxIP, which mediate the EB-dependent localization of +TIPs to growing microtubule ends.

In this study, we discovered and characterized a new EB-binding motif in Kar9. By combining biochemical, biophysical,

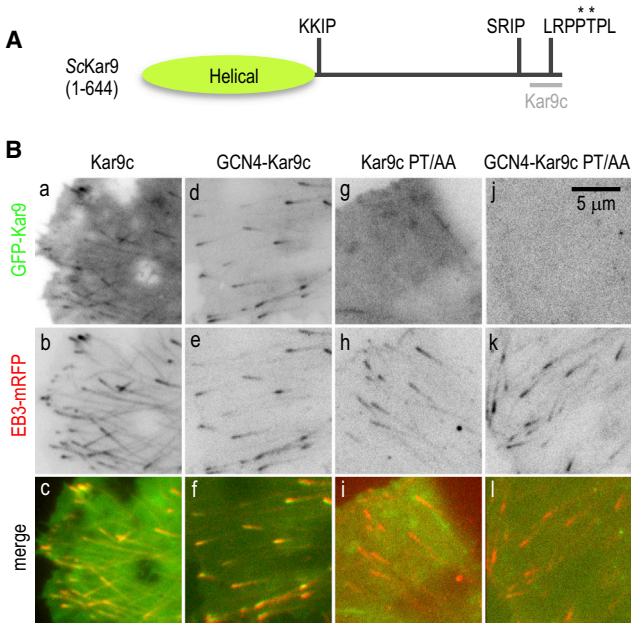


**Figure 1. Kar9c Tracks Growing Microtubule Ends in an EB-Dependent Manner**

(A) Locations of SxIP and LxxPTPh motifs in the C-terminal disordered region of Kar9. The N-terminal helical domain (residues 1–429) and the C-terminal disordered domain (residues 430–644) of ScKar9 are schematized with a green sphere and a black line, respectively. Kar9c (residues 594–644) is highlighted with a gray bar. The asterisks indicate the two residues, Pro624 and Thr625, which were simultaneously mutated in Kar9c to alanines (Kar9c-PT/AA).

(B) Localization of GFP-Kar9c (a–c), GFP-GCN4-Kar9c (d–f), GFP-Kar9c-PT/AA (g–i), and GFP-GCN4-Kar9c-PT/AA (j–l) in live COS-7 cells. Panels (a, d, g, j), (b, e, h, k), and (c, f, i, l) correspond to the GFP (Kar9c), mRFP (EB3), and the merged signals, respectively.

structural biology, and cell biology approaches, we found that the short linear motif LxxPTPh (where x and h represent any and hydrophobic amino acids, respectively) present in the C terminus of Kar9 binds the C-terminal domain of EB, and has the capacity to target a Kar9 fragment containing the motif to growing microtubule ends. The detailed structural and functional information gained on the EB-LxxPTPh interaction enabled us to discover LxxPTPh motifs in other +TIPs, suggesting that this distinct EB-binding element is a general feature of +TIP networks in many organisms.

## RESULTS

### The C Terminus of Kar9 Tracks Growing Microtubule Ends in an EB-Dependent Manner

We recently reported that the last 51 C-terminal residues (594–644) of *Saccharomyces cerevisiae* Kar9 (denoted as Kar9c) bind the C-terminal domain of the *S. cerevisiae* EB homolog Bim1 (denoted Bim1c), and that a conserved Pro624-Thr625 dipeptide within Kar9c is crucial for the Bim1c-Kar9c interaction (Figure 1A [Manatschal et al., 2016]). To test whether Kar9c C-terminally fused to GFP (GFP-Kar9c) is sufficient to target the protein chimera to growing microtubule ends, we performed live-cell imaging experiments. Since it is well known that dimerization can enhance the microtubule-tip tracking activity of SxIP-motif-containing polypeptides (Buey et al., 2012; Honnappa et al., 2009), we also tested a GCN4 leucine-zipper dimerized version of GFP-Kar9c (GFP-GCN4-Kar9c).

The microtubule-tip tracking activities of the two Kar9c constructs were subsequently tested in transfected COS-7 cells. We chose this cell type because its flat morphology allows the visualization of the microtubule cytoskeleton in a straightforward manner by live-cell imaging using total internal reflection fluorescence microscopy (TIRF [Komarova et al., 2009]). As shown in Figure 1Ba–c, expression of GFP-Kar9c resulted in a robust decoration of growing microtubule ends positive for EB3-mRFP, an activity that was further enhanced by dimerization (Figure 1Bd–f). Mutating the two residues Pro624 and Thr625 to alanine in both Kar9c variants (GFP-Kar9c-PT/AA and GFP-GCN4-Kar9c-PT/AA) abrogated the microtubule-tip tracking activity of the mutant proteins (Figure 1Bg–l), further underpinning the functional importance of the Pro624-Thr625 dipeptide (Manatschal et al., 2016). Collectively, these results demonstrate that the 50-amino-acid C-terminal disordered segment of Kar9 lacking any SxIP motifs, has the capacity to target a heterologous protein to growing microtubule ends.

### Kar9c Contains an LxxPTPh Motif that Binds the C-Terminal Domain of EBs

We sought to assess the importance of individual Kar9c residues for EB binding by using a synthetic peptide array on a cellulose membrane support (SPOT [Frank, 2002; Volkmer, 2009]). The peptide array shown in Figure 2A represents a complete amino acid substitution analysis of residue segment 610–633 of Kar9, in which all residues in this peptide were mutated, one at a time, to each of the 20 standard amino acids. The array was subsequently probed for His-Bim1 binding, which is reflected by black spots of variable intensities. Visual inspection of the SPOT array highlights the critical residues in Kar9c that are important for Bim1 binding. Based on this analysis, we derived the motif LxxPTPh (segment 621–627 of Kar9), where x represents any residue and h represents one of the hydrophobic amino acids Leu, Val, or Ile. Interestingly, this motif is highly conserved across budding yeast Kar9 orthologs, consistent with its high functional relevance (Figure 2B).

To determine the exact binding mode between the LxxPTPh motif of Kar9 and EB, we used X-ray crystallography. Structure solution of complexes between various Kar9c-derived peptides and constructs derived from Bim1c or the C-terminal domain of human EB1 (denoted EB1c) turned out to be difficult: only the apo Bim1c or EB1c structures were revealed each time in the obtained crystals. To overcome this problem, we used a fusion approach with the idea to link both components on the same polypeptide chain. To this end, we fused the Kar9 amino acid segment 615–633 (denoted Kar9c-p1) to the N terminus of an EB1c variant that lacks the 20 disordered C-terminal residues (denoted EB1cΔtail), and solved the structure of this chimeric protein to 2.3-Å resolution (Table 1). The crystals contained eight EB1cΔtail-Kar9c-p1 polypeptide fusions in their asymmetric unit. As expected, two EB1cΔtail monomers are respectively organized into coiled-coil dimers. In each of the four EB1cΔtail dimers, two Kar9c-p1 peptides are bound to the four-helix bundle EBH domain of EB1cΔtail (Figure 3A). The eight Kar9c-p1

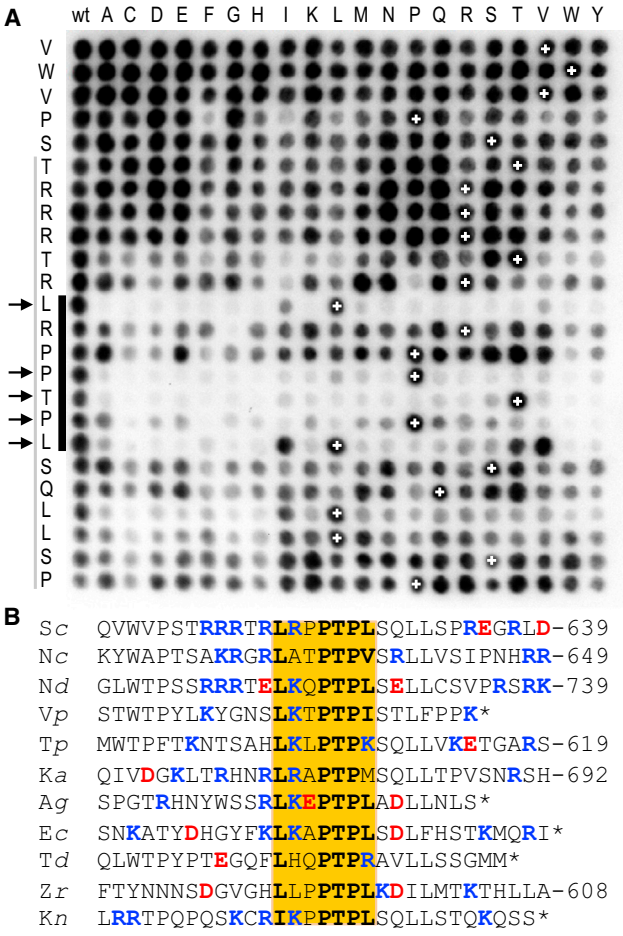


**Figure 2. SPOT Analysis of the Bim1-Kar9c Interaction**

(A) SPOT analysis of the Kar9 segment 610–633. Black spots indicate interaction between His-Bim1 and a membrane-bound Kar9c peptide. Each spot corresponds to a Kar9c variant peptide in which one residue of the Kar9c sequence (given on the left) was replaced by one of the 20 natural amino acids (shown on the top). The spots in the first column and the ones marked by white crosses represent replicas of the wild-type Kar9c sequence. The LxxPTPh motif and its critical residues are indicated on the left by a vertical bar and by arrows, respectively. The Kar9 peptide stretch (Kar9c-p1) incorporated in the EB1-Kar9c fusion and the LxxPTPh motif is indicated by a gray vertical bar.

(B) Multiple sequence alignment of budding yeast Kar9 paralogs highlighting the conservation of the LxxPTPh motif in the C terminus of the protein. Species are *Saccharomyces cerevisiae* (Sc), *Naumovozyma castellii* (Nc), *Naumovozyma dairenensis* (Nd), *Vanderwaltozyma polyspora* (Vp), *Tetrapisispora phaffii* (Tp), *Kazachstania africana* (Ka), *Ashbya gossypii* (Ag), *Eremothecium cymbalariae* (Ec), *Torulaspora delbrueckii* (Td), *Zygosaccharomyces rouxii* (Zr), and *Kazachstania naganishii* (Kn).

peptides present in the asymmetric unit assume a very similar EB1cΔtail-bound conformation (Figure S1A), suggesting a specific binding mode.

In the EB1cΔtail-Kar9c-p1 structure, we found well-defined electron densities and very similar main-chain and side-chain conformations for the segment 620-RLRPPTPL of all eight bound Kar9c-p1 peptides (average root-mean-square deviation [rmsd] of 0.34 Å over seven Cα atoms; Figures S1A and S1B). This result correlates well with the most sensitive region of Kar9c toward

**Table 1. X-Ray Data Collection and Refinement Statistics[a]**

| | |
|---|---|
| **Data Collection** | |
| Wavelength (Å) | 1.0 |
| Space group | $P12_11$ |
| Cell dimensions (Å) a, b, c | 42.35, 42.39,183.28 |
| α = γ, β (°) | 90, 90, 112.33 |
| Resolution (Å)[b] | 45.8–2.3 |
| Solvent content (%) | 49.29 |
| No. of unique reflections | 52,463 |
| I/σI | 16.4 (2.8) |
| Completeness (%) | 99.0 (97.3) |
| $R_{meas}$ (%) | 5.6 (50.1) |
| Multiplicity | 6.8 (6.4) |
| $CC_{1/2}$[c] | 99.9 (81.0) |
| **Refinement Statistics** | |
| $R_{work}/R_{free}$ (%) | 23.03/27.05 |
| No. of water molecules | 116 |
| Ramachandran statistics[d] | |
| Most favored (%) | 98.6 |
| Additionally allowed (%) | 1.4 |
| Disallowed (%) | 0.0 |
| Rmsd | |
| Bond lengths (Å) | 0.008 |
| Bond angles (°) | 1.16 |
| Mean atomic B values | |
| Protein atoms | 22.9 |

[a]Highest shell (2.4–2.3 Å) statistics are in parentheses.
[b]The resolution cutoff was selected based on I/σI and $CC_{1/2}$ according to Karplus and Diederichs (2012).
[c]$CC_{1/2}$ = percentage of correlation between intensities from random half-data sets (Karplus and Diederichs, 2012).
[d]As defined by MolProbity (Davis et al., 2004).

amino acid substitutions, segment 621–627, which encompasses the LxxPTPh motif (Figure 2A). As shown in Figure 3B, specific interactions between EB1cΔtail and Kar9c-p1 are mediated by both hydrophobic and polar residues. A prominent hydrophobic contact is formed by the Leu621 side chain of Kar9c-p1 (position 1 of LxxPTPh), which is deeply buried inside a hydrophobic cavity of the EBH domain shaped by residues Phe216′, Tyr217′, Phe218, Leu221, and Leu246 of EB1cΔtail (Figure 3C; primes discriminate residues stemming from the neighboring chain in the EB1cΔtail dimer). An electrostatic and hydrogen bonding network is further established between main-chain and side-chain atoms of Arg620, Pro624, Thr625, and Pro626 of Kar9c-p1 (positions −1, 4, 5, and 6 of LxxPTPh) and Asp209′, Glu213′, Tyr217′, Glu225, and Tyr247 of EB1cΔtail. Finally, Leu627 of Kar9c-p1 (position 7 of LxxPTPh) is in van der Waals distance from Thr206′, Val207, and Leu210′ of EB1c. Notably, all EB1cΔtail residues that are in direct contact with Kar9c-p1 are highly conserved among EB orthologs (Figure S1C). Conversely, all key residues of Kar9c-p1 that follow the LxxPTPh motif (i.e., Leu621, Pro624, Thr625, Pro626, and Leu627) are involved in specific interactions with the EBH domain.

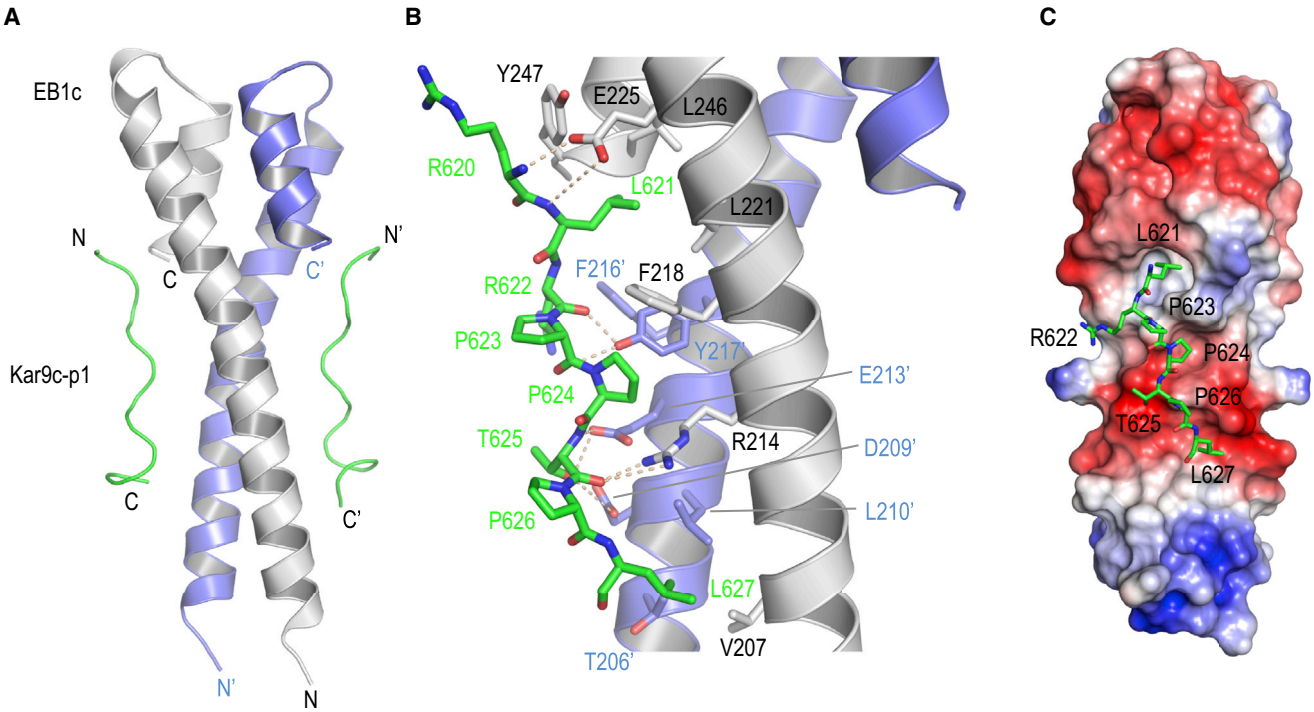


**Figure 3. Crystal Structure of the EB1c-Kar9c-p1 Complex**

(A) Overall crystal structure of the EB1cΔtail-Kar9c-p1 complex. The two monomers of the EB1cΔtail homodimer are shown in cartoon representation and are colored gray and light blue, respectively. The two Kar9c-p1 peptides are shown in ribbon representation and are colored green.

(B) Close-up view of the EB1cΔtail-Kar9c-p1 interaction. Same color code as in (A). Kar9c-p1 is depicted in sticks representation. Oxygen and nitrogen atoms are colored red and blue, respectively. Hydrogen bonds are depicted as gray broken lines, and key residues of EB1cΔtail and Kar9c-p1 are labeled.

(C) Surface view of EB1cΔtail color coded with the electrostatic potential (from −15 to +15 kBT; red and blue depict negative and positive electrostatic potentials, respectively). Kar9c-p1 is shown in sticks representation as in (B).

See also Figures S1 and S4.

To probe the interaction between Kar9c-p1 and full-length human EB1 in solution, we performed isothermal titration calorimetry (ITC) experiments. As shown in Figure S1D, two Kar9c-p1 peptides bound to one EB1 dimer with an equilibrium dissociation constant, $K_D$, of 4.5 ± 0.2 μM. The EB1cΔtail-Kar9c-p1 structure shows that Tyr217 and Glu225 of EB1 establish five hydrogen bonds with the LxxPTPh motif of Kar9c-p1. Simultaneous mutation of Tyr217 and Glu225 to alanines (EB1-YE/AA) essentially abrogated the interaction of the mutant domain to Kar9c-p1 (Figure S1D), demonstrating their key role in LxxPTPh binding.

Collectively, these results establish that the highly conserved EBH domain of EBs is an LxxPTPh motif recognition domain.

## The C-Terminal Tail Region of EB Is Dispensable for EB-LxxPTPh Complex Formation

It is well established that the C-terminal disordered tail of EB1 becomes structured upon SxIP binding and is important for EB-SxIP complex formation (Honnappa et al., 2009; Montenegro Gouveia et al., 2010). Similarly, productive binding of CAP-Gly domains relies on the very C-terminal EEY/F motif of EBs (Honnappa et al., 2006; Weisbrich et al., 2007). In our EB1cΔtail-Kar9c-p1 structure, we used an EB1c variant that lacks the entire tail region. The structure may thus indicate that this EB1c segment, in contrast to SxIP and CAP-Gly, is dispensable for LxxPTPh binding. To test this hypothesis, we performed interaction studies with Bim1c and Kar9c-p1 using ITC. As shown in Figure 4A, two Kar9c-p1 peptides bound to one Bim1c dimer with a $K_D$ of 1.3 ± 0.12 μM. A very similar affinity of 1.5 ± 0.19 μM was obtained for a Bim1c truncation mutant that lacked the C-terminal tail region (Bim1cΔtail). These results demonstrate that the EB tails are indeed dispensable for LxxPTPh binding. Interestingly, this observation is in contrast to what we obtained with an SxIP-motif-containing peptide derived from the human microtubule-actin crosslinking factor 1 (MACF1-p2), which failed to interact with Bim1cΔtail (Figure 4A), consistent with previous findings (Montenegro Gouveia et al., 2010). These data suggest that the EB-binding mechanisms of LxxPTPh and SxIP are different.

To test whether the tail region of EB is also dispensable for recruiting LxxPTPh-motif-containing proteins to growing microtubule tips, we performed in vitro reconstitution assays. We used GFP-Kar9c and combined it with either mCherry-labeled wild-type EB3 (mCherry-EB3) or a mutant thereof that lacked the tail region (mCherry-EB3Δtail [Montenegro Gouveia et al., 2010]). As shown in Figures 4B and 4C, GFP-Kar9c tracked growing microtubule ends in the presence of mCherry-EB3Δtail to a similar extent as with mCherry-EB3. In contrast, no

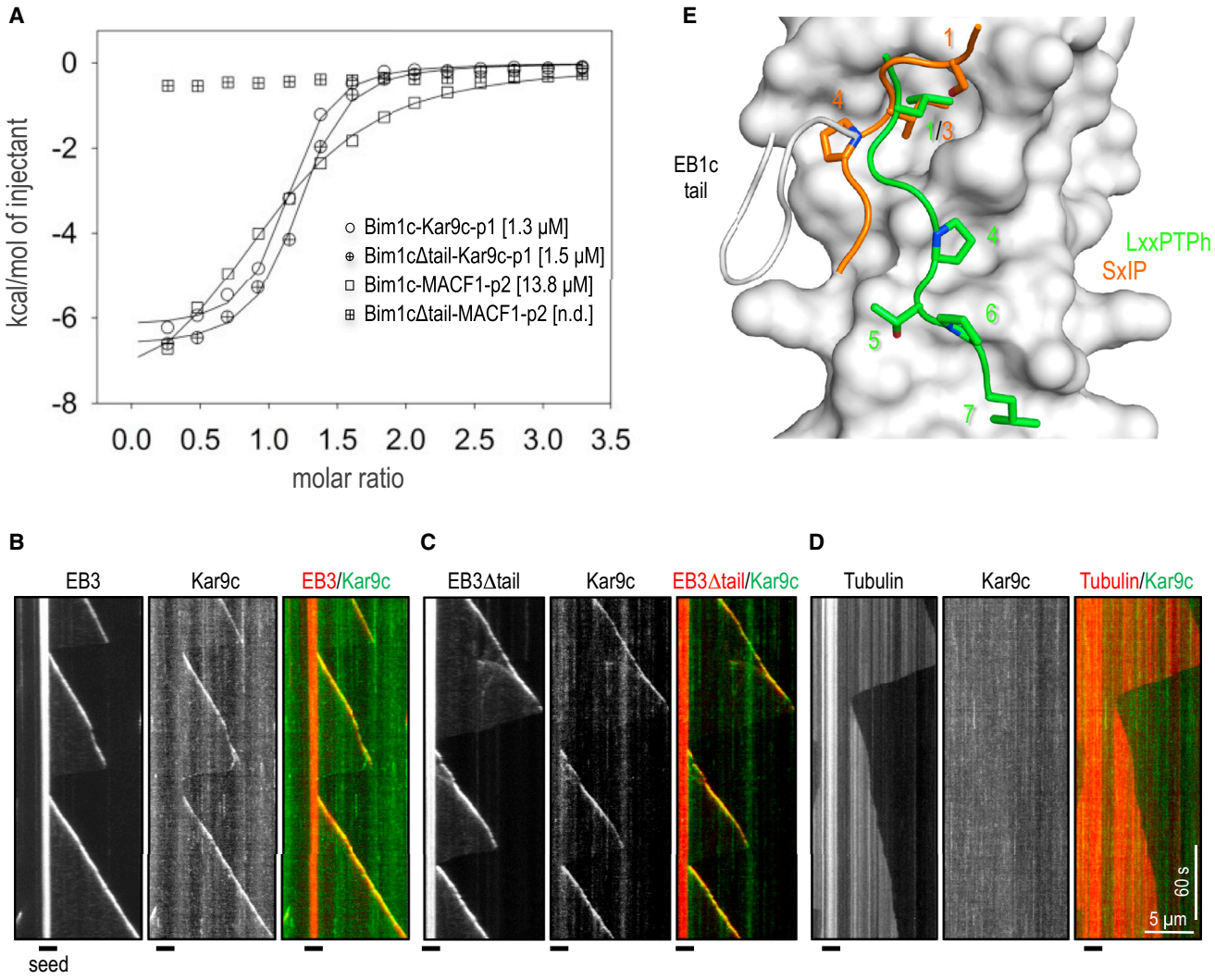


**Figure 4. Comparison of the EB-SxIP and EB-LxxPTPh Interaction Modes**

(A) Binding isotherms determined by ITC for the Bim1c-Kar9c-p1, Bim1cΔtail-Kar9c-p1, Bim1c-MACF1-p2, and Bim1cΔtail-MACF1-p2 interactions. Derived $K_D$ values are indicated in parentheses. n.d., not determined.

(B–D) Kymographs showing the microtubule tip tracking behavior of GFP-Kar9c (0.64 μM, green) in in vitro reconstitution assays on dynamic microtubules grown from rhodamine-tubulin-labeled seeds in the presence of tubulin (15 μM) and mCherry-EB3 or mCherry-EB3Δtail (B and C, respectively; 20 nM each, red), or in the absence of EB (D). In the experiment shown in (D), 0.5 μM rhodamine-tubulin was added to the reaction mixture.

(E) Superimposition of the EB1cΔtail-Kar9c-p1 and EB1cΔC8-MACFp1 (PDB: 3GJO) complex structures. EB1c is depicted in light-gray surface representation; the C-terminal tail region that is only structured in the EB1c-SxIP complex is shown in cartoon representation. The LxxPTPh (green) and SxIP (orange) motifs are shown as cartoons with key residues in sticks representation. Numbers refer to the position of residues in the corresponding motifs. The motif sequences shown on the right have been aligned according to their structural superimposition.

See also Figures S2 and S3.

microtubule-tip tracking of GFP-Kar9c was observed in the absence of any EB3 protein (Figure 4D). To test whether human EB3 can be replaced by an EB from a different species, we performed a reconstitution with the fission yeast EB ortholog Mal3 (Bieling et al., 2007). Similar to EB3, Mal3 readily recruited GFP-Kar9c to growing microtubule ends (Figure S2A). These results demonstrate that the C-terminal tail region of EB is dispensable for recruiting LxxPTPh-motif containing +TIPs to growing microtubule tips. They further show that the microtubule-tip tracking activity of LxxPTPh proteins does not depend on a particular EB ortholog, suggesting a conserved mechanism across eukaryotes.

Next, we compared the EB-LxxPTPh and EB-SxIP (Honnappa et al., 2009) binding modes. Superimposition of the two structures revealed that both LxxPTPh- and SxIP-containing peptides display the same Nter → Cter sequence polarity with respect to their binding sites (Figure 4E). The superimposition further revealed that the two motifs bind one common and several distinct structural elements present on the surface of the EBH domain. The common interaction point is mediated by the hydrophobic

leucine and isoleucine residues at positions 1 and 3 of the LxxPTPh and SxIP motifs, respectively, whose corresponding side chains insert into the hydrophobic cavity of the EBH domain in a similar manner (Figure 4E). The remaining key residues of both motifs, however, bind to completely different regions on the EBH domain. While the serine residue at position 1 of SxIP is engaged with residues shaping the hydrophobic cavity of the EBH domain, the two prolines, threonine and leucine residues at positions 4–7 of LxxPTPh, interact with residues exposed on the surface and at the interface between the two coiled-coil monomers of the EBH domain (Figures 3B and 4E). Notably, the presence of an arginine residue at position 2 of LxxPTPh, which corresponds to the critical proline at position 4 of SxIP, would clash into the surface of the EB1c domain if the flexible C-terminal tail of EB1c were to fold in an equivalent manner as seen in the EB-SxIP complex structure (Figure S3A). While this analysis does not exclude that the EB1c tail region could engage the LxxPTPh peptide, it does not significantly contribute to the affinity of the EB-LxxPTPh interaction based on our ITC data (Figure 4A).

To test whether LxxPTPh and SxIP compete for binding to EBs as predicted by our structural analysis, we performed fluorescence polarization competition experiments. We found that an LxxPTPh-containing Kar9 fragment fused C-terminally to thioredoxin (Manatschal et al., 2016) could fully displace a Bim1 pre-bound and fluorescein-labeled SxIP-containing peptide derived from MACF1 (FC-MACF-p1 [Buey et al., 2012]; Figure S3B). This result underpins the validity of our structural analysis of the EB-LxxPTPh and EB-SxIP complexes (Figure 4E).

Positively charged residues present within or in the flanking regions of SxIP motifs are known to interact with the negatively charged surface of the C-terminal EB domain, thus contributing to the overall stability of the EB-SxIP complex (Buey et al., 2011, 2012; Honnappa et al., 2009). As highlighted in Figure 2B, several positively charged residues are also found within and near the LxxPTPh motif of Kar9 orthologs. To test whether charged residues contribute to the affinity of the Bim1c-LxxPTPh interaction, we performed ITC experiments with Bim1c and Kar9c in the presence of increasing amounts of sodium chloride in the buffer (150–800 mM). As shown in Figure S2B, we indeed found that the stability of the Bim1c-Kar9c complex is salt dependent. Inspection of the electrostatic surface potential of the EB1cΔtail-Kar9c-p1 structure reveals that positively charged residues on the N-terminal side or within the LxxPTPh motif could indeed stabilize the complex via long-range, unspecific electrostatic attractive interactions with the negatively charged surface of the EBH domain (Figure 3C).

Collectively, these results demonstrate that in contrast to SxIP and CAP-Gly, the EB-binding mechanism of LxxPTPh does not involve the C-terminal tail region of EBs. They further demonstrate that binding of LxxPTPh and SxIP to the C-terminal domain of EBs is mutually exclusive and is regulated by electrostatic attractive interactions.

### LxxPTPh Motifs Are Found in Diverse Mammalian +TIPs

We sought to assess whether LxxPTPh motifs in other +TIPs besides Kar9 can mediate microtubule plus-end tracking. To this end we used the structural and functional information gained so far to screen a human EB pull-down-based mass spectrometry sequence database (Jiang et al., 2012). A list of sequences was assembled based on a manual search of proteins that (1) contain the motif in a predicted unstructured sequence region of the protein candidate, (2) show zero or one residue deviation at positions 1, 4, 5, 6, or 7 of the LxxPTPh motif, and (3) display positively charged residues preferentially at positions 2 and 3 or on the N-terminal side of the motif. The protein candidates that we selected for further investigation are the human proteins TACC1, MACF1 (sites 1 and 2), SLAIN1, Pumilio, PDZRN4, and PDZDCP (Figures 5A and 5B).

To test the activities of the selected sequences, we fused 50-amino-acid stretches encompassing the different LxxPTPh motifs C-terminally to GFP-GCN4 and analyzed the localization of the resulting chimeric proteins in COS-7 cells. Interestingly, the wild-type TACC1, MACF1 site 2, and SLAIN1 chimera tracked growing microtubule ends (Figures 5Ca–c, 5Da–c, and 5Ea–c); for MACF1 site 1, Pumilio, PDZRN4, and PDZDCP no localization to microtubule tips was observed (not shown). To test the functionality of the identified microtubule plus-end tracking LxxPTPh motifs, we substituted the residues at positions 4 and 5 of the corresponding LxxPTPh motifs in each chimera to alanines. As shown in Figures 5Dd–f and 5Ed–f, the mutant TACC1 and MACF1 site 2 chimera failed to track microtubule tips. In the case of the SLAIN1 mutant chimera, the tip tracking activity was diminished but not abrogated (Figure 5Cd–f). Inspection of the corresponding sequence revealed that the SLAIN1 fusion peptide contains an SxIP motif (SNLP) on the N-terminal side of its LxxPTPh motif (Figure 5B). To test whether this sequence stretch contributes to the microtubule-tip tracking activity of the SLAIN1 peptide, we substituted the residues at positions 2 and 3 of the SxIP motif to alanines both in the wild-type and LxxPTPh mutant background. As shown in Figure 5Cg–l, while the SxIP mutant SLAIN1 chimera (SLAIN1 LP/AA) still displayed a decreased but robust microtubule-tip tracking activity, the double SxIP and LxxPTPh mutant (SLAIN1 [LP/AA-PK/AA]) failed to do so. Notably, the tandem occurrence of SxIP and LxxPTPh, like in SLAIN1, is also observed in Kar9 (Manatschal et al., 2016). This observation highlights that both SxIP and LxxPTPh motifs can occur and cooperate in the same protein.

Why did the peptides derived from MACF1 site 1, Pumilio, PDZRN4, and PDZDCP not localize to microtubule tips? Inspection of the corresponding sequences reveals that in contrast to the positive hits, these sequences display a reduced number of positively charged residues on the N-terminal side or at positions 2 and 3 of the corresponding LxxPTPh motifs (Figure 5A). In the case of MACF site 1, which otherwise contains an adequate number of positively charged residues, the four consecutive prolines on the C-terminal side of LxxPTPh (LSQPTPPPMP) may sterically hinder the peptide to properly engage with its binding site. Collectively, these observations emphasize that sequence context is critical for the activity of LxxPTPh motifs.

## DISCUSSION

Until now, CAP-Gly domains and SxIP motifs were the only known elements that mediate +TIP interactions with EBs. Here, we expanded the repertoire of EB-binding elements by demonstrating that a novel LxxPTPh motif embedded in a disordered and basic sequence region enables diverse +TIPs to access the

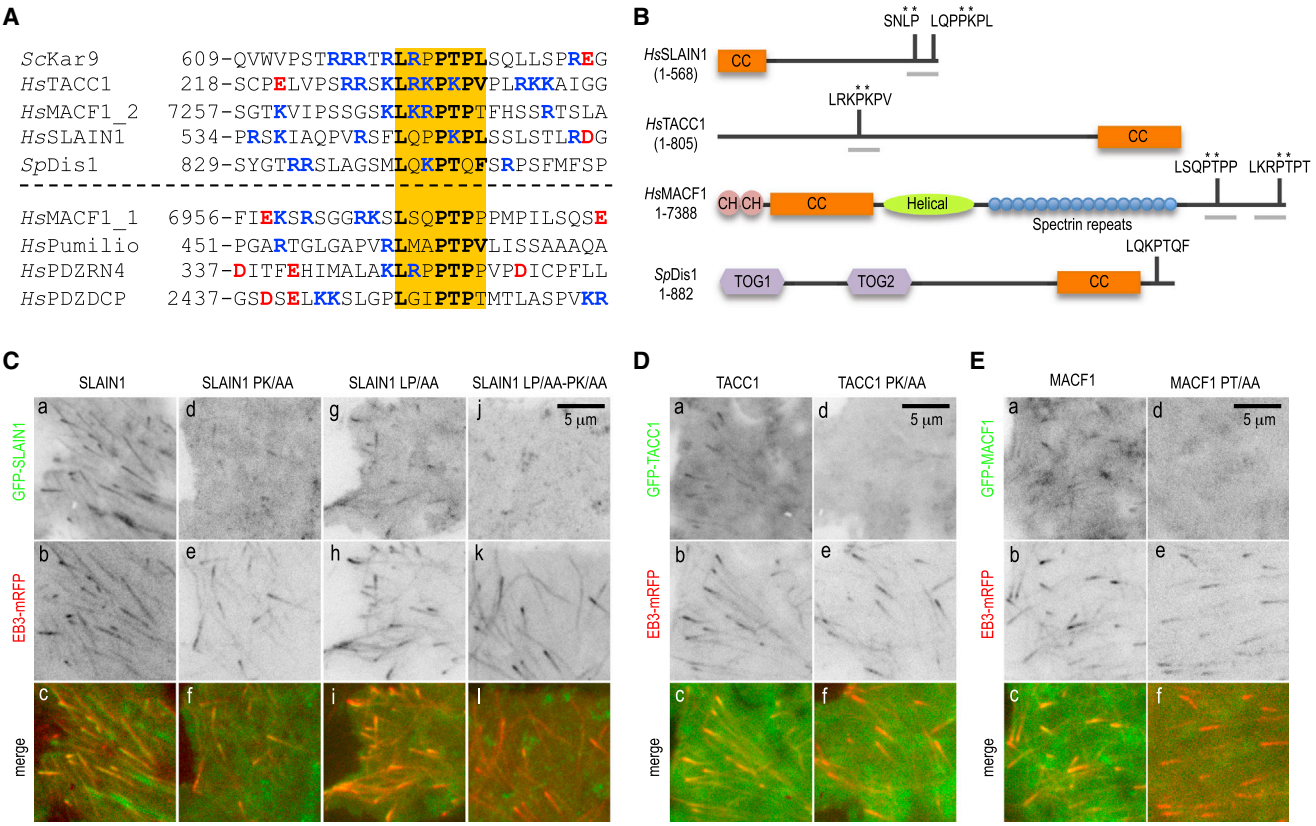


**Figure 5. Identification of Functional LxxPTPh Motifs in Other +TIPs**

(A) Multiple sequence alignment of the sequence region around LxxPTPh motifs in the human +TIP candidate TACC1, MACF1 (site 1 and site 2), SLAIN1, Pumilio, PDZRN4, and PDZDCP, and in the *S. pombe* +TIP Dis1.

(B) Location of LxxPTPh and SxIP motifs in Kar9, SLAIN1, TACC1, MACF1 site 2, and Dis1. Orange rectangle, coiled-coil domain; green oval, helical domain; pink sphere, CH domain; blue sphere, spectrin repeat; purple hexagon, TOG domain; black line, basic/serine-rich disordered region. The gray bars represent the LxxPTPh-motif-containing sequence stretches that were tested as GFP-fusion proteins in COS-7 cells; the asterisks indicate the SxIP and LxxPTPh motif residues that were simultaneously mutated to alanines.

(C–E) Localization of GFP-GCN4-SLAIN1 (amino acids [aa] 516–568) (C [a–c]), GFP-GCN4-TACC1 (aa 201–254) (D [a–c]), GFP-GCN4-MACF1 (aa 7,257–7,314) (E [a–c]), GFP-GCN4-SLAIN1 PK/AA (aa 516–568) (C [d–f]), GFP-GCN4-SLAIN1 LP/AA (aa 516–568) (C [g–i]), GFP-GCN4-SLAIN1 PK/AA-LP/AA (aa 516–568) (C [j–l]), GFP-GCN4-TACC1 PK/AA (aa 201–254) (D [d–f]), and GFP-GCN4-MACF1 PT/AA (aa 7,257–7,314) (E [d–f]) in live COS-7 cells. The panels C (a, d, g, j), D (a, d), E (a, d), C (b, e, h, k), D (b, e), E (b, e), C (c, f, I, l), D (c, f), and E (c, f) correspond to the GFP (+TIP chimera), mRFP (EB3), and merged signals, respectively.

growing ends of microtubules by directly interacting with EBs. Importantly, the C-terminal tail region of EB is dispensable for its interaction with LxxPTPh. This is in contrast to SxIP and CAP-Gly, which fully depend on this EB segment for productive complex formation and localization to microtubule tips (Honnappa et al., 2006, 2009; Montenegro Gouveia et al., 2010; Weisbrich et al., 2007). One immediate implication of this result is that EB versions that lack the C-terminal tails cannot be used to abrogate the localization behavior of all EB-dependent +TIPs in cells (Gierke and Wittmann, 2012). We also note that our previous EB pull-down/mass spectrometry +TIP candidate list, which was obtained with full-length EBs, most likely is biased toward SxIP- and CAP-Gly-containing +TIPs (Jiang et al., 2012). The results presented here will allow modifying our approach with the aim to identify LxxPTPh-motif-containing +TIPs in entire genomes.

The detailed molecular information obtained on Kar9c enabled us to discover additional +TIPs that contain functional LxxPTPh motifs. Furthermore, while our manuscript was in preparation the molecular mechanism of interaction between the fission yeast proteins Mal3 and Dis1 (ortholog of XMAP215/chTOG) was published by another group (Matsuo et al., 2016). The binding mode of EB1-Kar9c described by us is very similar to that observed in the complex formed between residues 841-LQKPTQF of Dis1 and the EBH domain of Mal3 (Figure S4 [Matsuo et al., 2016]). Notably, this Dis1 sequence, with the exception of the motif position 6 residue (glutamine instead of proline), matches the LxxPTPh motif signature (Figures 5A and 5B), thus further extending the repertoire of proteins containing this +TIP element. Collectively, these results establish LxxPTPh as a novel type and general "Microtubule tip Localization Signal" (MtLS [Honnappa et al., 2009]) besides SxIP.

What is the functional significance of having two different linear +TIP motifs with similar EB-binding activities? An immediate benefit, for example, of having LxxPTPh and SxIP arranged in tandem and separated by a few tens of residues, as is the case for Kar9 and SLAIN1, is a significant gain in affinity toward a single EB dimer (two to three orders of magnitude in the case of

Bim1-Kar9 [Manatschal et al., 2016]). However, our finding that LxxPTPh and SxIP differentially depend on the C-terminal tail region of EBs suggests that they can mediate different types of hierarchical +TIP network topologies. While interaction of SxIP with EB is known to compete with CAP-Gly binding (Duellberg et al., 2014), the EB-LxxPTPh interaction is not expected to significantly interfere with such a higher-order EB complex formation. A second possibility is differential regulation. We recently reported that the SxIP-like and LxxPTPh motifs of Kar9 are inactive during spindle positioning in metaphase, most likely due to phosphorylation events, while its canonical SxIP motif is fully functional in this particular cell-cycle stage (Manatschal et al., 2016). Furthermore, acetylation of Lys220 of EB1 has been shown to modulate the interaction of EB1 with SxIP proteins (Xia et al., 2012). Based on structural considerations, Lys220 seems important to stabilize a favorable conformation of the EB1 tail for productive SxIP binding, and acetylation of its side chain may hinder this molecular process (Honnappa et al., 2009; Xia et al., 2012). Since the EB-tail conformation is not critical for LxxPTPh binding, we expect that acetylation of Lys220 will not significantly influence EB-LxxPTPh complex formation.

Taken together, the detailed molecular knowledge about LxxPTPh motifs presented and discussed in this study sets the stage to identify new +TIPs with unexplored functions. It further provides a framework to understand the hierarchical nature, organization, and regulation of +TIP networks for controlling the fate of microtubule tips in central cellular processes.

## STAR★METHODS

Detailed methods are provided in the online version of this paper and include the following:

- KEY RESOURCES TABLE
- CONTACT FOR REAGENT AND RESOURCE SHARING
- METHOD DETAILS
  - Protein and Peptide Preparation
  - Isothermal Titration Calorimetry (ITC)
  - Fluorescence Polarization Spectroscopy
  - X-Ray Crystallography
  - Microtubule Tip Tracking Reconstitution Assay
  - Synthetic Peptide Arrays on Cellulose Membranes (SPOT)
  - Constructs, Cell Culture and Transfection
  - Image Acquisition
- DATA AND SOFTWARE AVAILABILITY

## SUPPLEMENTAL INFORMATION

Supplemental Information includes four figures and can be found with this article online at http://dx.doi.org/10.1016/j.str.2017.04.010.

## AUTHOR CONTRIBUTIONS

A.K., C.M., A.R., I.G., M.S.D., R.V., R.A.K., A.A., and M.O.S. designed the research. A.K., C.M., A.R., I.G., M.S.D., R.J., and I.K. performed the research. A.K., C.M., A.R., I.G., M.S.D., A.E.P., R.V., A.A., and M.O.S. analyzed the data. A.K. and M.O.S. wrote the paper with input from all the authors.

## ACKNOWLEDGMENTS

We are indebted to Kai Jiang for help with mass spectrometry database searches, to Daniel Frey for support with protein purification, and to Vincent Olieric and Meitian Wang for excellent technical assistance at the synchrotron beamlines. The X-ray data were collected at beamline X06DA of the Swiss Light Source (Paul Scherrer Institut, Villigen, Switzerland). This work was supported by a Marie Curie COFUND fellowship (to A.K.), and by grants from the Netherlands Organisation for Scientific Research (NWO) CW ECHO (711.015.005; to A.A.), from the Swiss National Science Foundation (310030B_138659 and 31003A_166608; to M.O.S.), and from SystemsX.ch (RTD-TubeX; to M.O.S.).

Received: February 20, 2017
Revised: April 6, 2017
Accepted: April 28, 2017
Published: May 25, 2017

## REFERENCES

Akhmanova, A., and Steinmetz, M.O. (2015). Control of microtubule organization and dynamics: two ends in the limelight. Nat. Rev. Mol. Cell Biol. *16*, 711–726.

Bieling, P., Laan, L., Schek, H., Munteanu, E.L., Sandblad, L., Dogterom, M., Brunner, D., and Surrey, T. (2007). Reconstitution of a microtubule plus-end tracking system in vitro. Nature *450*, 1100–1105.

Bjelic, S., De Groot, C.O., Scharer, M.A., Jaussi, R., Bargsten, K., Salzmann, M., Frey, D., Capitani, G., Kammerer, R.A., and Steinmetz, M.O. (2012). Interaction of mammalian end binding proteins with CAP-Gly domains of CLIP-170 and p150(glued). J. Struct. Biol. *177*, 160–167.

Buey, R.M., Mohan, R., Leslie, K., Walzthoeni, T., Missimer, J.H., Menzel, A., Bjelic, S., Bargsten, K., Grigoriev, I., Smal, I., et al. (2011). Insights into EB1 structure and the role of its C-terminal domain for discriminating microtubule tips from the lattice. Mol. Biol. Cell *22*, 2912–2923.

Buey, R.M., Sen, I., Kortt, O., Mohan, R., Gfeller, D., Veprintsev, D., Kretzschmar, I., Scheuermann, J., Neri, D., Zoete, V., et al. (2012). Sequence determinants of a microtubule tip localization signal (MtLS). J. Biol. Chem. *287*, 28227–28242.

Collaborative Computational Project, Number 4 (1994). The CCP4 suite: programs for protein crystallography. Acta Cryst. *D50*, 760–763.

Davis, I.W., Murray, L.W., Richardson, J.S., and Richardson, D.C. (2004). MOLPROBITY: structure validation and all-atom contact analysis for nucleic acids and their complexes. Nucleic Acids Res. *32*, W615–W619.

Doodhi, H., Prota, A.E., Rodríguez-García, R., Xiao, H., Custar, D.W., Bargsten, K., Katrukha, E.A., Hilbert, M., Hua, S., Jiang, K., et al. (2016). Termination of protofilament elongation by eribulin induces lattice defects that promote microtubule catastrophes. Curr. Biol. *26*, 1713–1721.

Duellberg, C., Trokter, M., Jha, R., Sen, I., Steinmetz, M.O., and Surrey, T. (2014). Reconstitution of a hierarchical +TIP interaction network controlling microtubule end tracking of dynein. Nat. Cell Biol. *16*, 804–811.

Emsley, P., and Cowtan, K. (2004). Coot: model-building tools for molecular graphics. Acta Crystallogr. D. Biol. Crystallogr. *60*, 2126–2132.

Frank, R. (2002). The SPOT-synthesis technique. Synthetic peptide arrays on membrane supports–principles and applications. J. Immunol. Methods *267*, 13–26.

Galjart, N. (2010). Plus-end-tracking proteins and their interactions at microtubule ends. Curr. Biol. *20*, R528–R537.

Gierke, S., and Wittmann, T. (2012). EB1-recruited microtubule +TIP complexes coordinate protrusion dynamics during 3D epithelial remodeling. Curr. Biol. *22*, 753–762.

Honnappa, S., John, C.M., Kostrewa, D., Winkler, F.K., and Steinmetz, M.O. (2005). Structural insights into the EB1-APC interaction. EMBO J. *24*, 261–269.

Honnappa, S., Okhrimenko, O., Jaussi, R., Jawhari, H., Jelesarov, I., Winkler, F.K., and Steinmetz, M.O. (2006). Key interaction modes of dynamic +TIP networks. Mol. Cell *23*, 663–671.

Honnappa, S., Gouveia, S.M., Weisbrich, A., Damberger, F.F., Bhavesh, N.S., Jawhari, H., Grigoriev, I., van Rijssel, F.J., Buey, R.M., Lawera, A., et al. (2009).

An EB1-binding motif acts as a microtubule tip localization signal. Cell *138*, 366–376.

Jiang, K., Toedt, G., Montenegro Gouveia, S., Davey, N.E., Hua, S., van der Vaart, B., Grigoriev, I., Larsen, J., Pedersen, L.B., Bezstarosti, K., et al. (2012). A proteome-wide screen for mammalian SxIP motif-containing microtubule plus end tracking proteins. Curr. Biol. *22*, 1800–1807.

Kabsch, W. (2010). XDS. Acta Crystallogr. D. Biol. Crystallogr. *66*, 125–132.

Karplus, P.A., and Diederichs, K. (2012). Linking crystallographic model and data quality. Science *336*, 1030–1033.

Komarova, Y., De Groot, C.O., Grigoriev, I., Gouveia, S.M., Munteanu, E.L., Schober, J.M., Honnappa, S., Buey, R.M., Hoogenraad, C.C., Dogterom, M., et al. (2009). Mammalian end binding proteins control persistent microtubule growth. J. Cell Biol. *184*, 691–706.

Korinek, W.S., Copeland, M.J., Chaudhuri, A., and Chant, J. (2000). Molecular linkage underlying microtubule orientation toward cortical sites in yeast. Science *287*, 2257–2259.

Kumar, P., and Wittmann, T. (2012). +TIPs: SxIPping along microtubule ends. Trends Cell Biol. *22*, 418–428.

Kurihara, L.J., Beh, C.T., Latterich, M., Schekman, R., and Rose, M.D. (1994). Nuclear congression and membrane fusion: two distinct events in the yeast karyogamy pathway. J. Cell Biol. *126*, 911–923.

Laskowski, R.A., MacArthur, M.W., Moss, D.S., and Thornton, J.M. (1993). PROCHECK: a program to check the stereochemical quality of protein structures. J. Appl. Cryst. *26*, 283–291.

Liakopoulos, D., Kusch, J., Grava, S., Vogel, J., and Barral, Y. (2003). Asymmetric loading of Kar9 onto spindle poles and microtubules ensures proper spindle alignment. Cell *112*, 561–574.

Manatschal, C., Farcas, A.M., Degen, M.S., Bayer, M., Kumar, A., Landgraf, C., Volkmer, R., Barral, Y., and Steinmetz, M.O. (2016). Molecular basis of Kar9-Bim1 complex function during mating and spindle positioning. Mol. Biol. Cell *27*, 3729–3745.

Matsuo, Y., Maurer, S.P., Yukawa, M., Zakian, S., Singleton, M.R., Surrey, T., and Toda, T. (2016). An unconventional interaction between Dis1/TOG and Mal3/EB1 in fission yeast promotes the fidelity of chromosome segregation. J. Cell Sci. *129*, 4592–4606.

McCoy, A.J., Grosse-Kunstleve, R.W., Adams, P.D., Winn, M.D., Storoni, L.C., and Read, R.J. (2007). Phaser crystallographic software. J. Appl. Crystallogr. *40*, 658–674.

Miller, R.K., and Rose, M.D. (1998). Kar9p is a novel cortical protein required for cytoplasmic microtubule orientation in yeast. J. Cell Biol. *140*, 377–390.

Molk, J.N., Salmon, E.D., and Bloom, K. (2006). Nuclear congression is driven by cytoplasmic microtubule plus end interactions in *S. cerevisiae*. J. Cell Biol. *172*, 27–39.

Montenegro Gouveia, S., Leslie, K., Kapitein, L.C., Buey, R.M., Grigoriev, I., Wagenbach, M., Smal, I., Meijering, E., Hoogenraad, C.C., Wordeman, L., et al. (2010). In vitro reconstitution of the functional interplay between MCAK and EB3 at microtubule plus ends. Curr. Biol. *20*, 1717–1722.

Murshudov, G.N., Vagin, A.A., and Dodson, E.J. (1997). Refinement of macromolecular structures by the maximum-likelihood method. Acta Cryst. *D53*, 240–255.

O'Shea, E.K., Klemm, J.D., Kim, P.S., and Alber, T. (1991). X-ray structure of the GCN4 leucine zipper, a two-stranded, parallel coiled coil. Science *254*, 539–544.

Olieric, N., Kuchen, M., Wagen, S., Sauter, M., Crone, S., Edmondson, S., Frey, D., Ostermeier, C., Steinmetz, M.O., and Jaussi, R. (2010). Automated seamless DNA co-transformation cloning with direct expression vectors applying positive or negative insert selection. BMC. Biotechnol. *10*, 56.

Painter, J., and Merritt, E.A. (2006). TLSMD web server for the generation of multi-group TLS models. J. Appl. Crystallogr. *39*, 109–111.

Slep, K.C. (2010). Structural and mechanistic insights into microtubule end-binding proteins. Curr. Opin. Cell Biol. *22*, 88–95.

Slep, K.C., Rogers, S.L., Elliott, S.L., Ohkura, H., Kolodziej, P.A., and Vale, R.D. (2005). Structural determinants for EB1-mediated recruitment of APC and spectraplakins to the microtubule plus end. J. Cell Biol. *168*, 587–598.

Volkmer, R. (2009). Synthesis and application of peptide arrays: quo vadis SPOT technology. Chembiochem *10*, 1431–1442.

Weisbrich, A., Honnappa, S., Jaussi, R., Okhrimenko, O., Frey, D., Jelesarov, I., Akhmanova, A., and Steinmetz, M.O. (2007). Structure-function relationship of CAP-Gly domains. Nat. Struct. Mol. Biol. *14*, 959–967.

Wenschuh, H., Volkmer-Engert, R., Schmidt, M., Schulz, M., Schneider-Mergener, J., and Reineke, U. (2000). Coherent membrane supports for parallel microsynthesis and screening of bioactive peptides. Biopolymers *55*, 188–206.

Xia, P., Wang, Z., Liu, X., Wu, B., Wang, J., Ward, T., Zhang, L., Ding, X., Gibbons, G., Shi, Y., and Yao, X. (2012). EB1 acetylation by P300/CBP-associated factor (PCAF) ensures accurate kinetochore-microtubule interactions in mitosis. Proc. Natl. Acad. Sci. USA *109*, 16564–16569.

## STAR★METHODS

### KEY RESOURCES TABLE

| REAGENT or RESOURCE | SOURCE | IDENTIFIER |
|---|---|---|
| Antibodies | | |
| Mouse anti polyhistidine IgG | Sigma H-1029 | www.sigmaaldrich.com |
| Horseradish-peroxidase conjugated anti-mouse IgG | Sigma A-5906 | www.sigmaaldrich.com |
| Bacterial and Virus Strains | | |
| E. coli BL21 (DE3) | Stratagene | www.agilent.com |
| Chemicals, Peptides, and Recombinant Proteins | | |
| EB1c-Kar9c-p1 (residues 191-248 of human EB1 and residues 615-633 of *S. cerevisiae* Kar9; UniProtKB ID P32526) | This study | |
| GFP-Kar9c (residues 594-644 of Kar9) | This study | |
| mCherry-EB3 | This study | |
| mCherry-EB3Δtail | This study | |
| human EB1 (residues 1-268) | This study | |
| EB1-YE/AA (residues 1-268) | This study | |
| Trx-Kar9-Site2 | Manatschal et al., 2016 | |
| Trx-Kar9-Site3 | Manatschal et al., 2016 | |
| Bim1 (residues 1-344) | This study | |
| Bim1c (residues 183-344) | This study | |
| Bim1cΔtail (residues 183-274) | This study | |
| Mal3-GFP | Manatschal et al., 2016 | |
| Kar9c-p1 peptide (TRRRTRLRPPTPLSQLLSP) | This study | |
| FC-MACF1-p1 peptide (HRPTPRAGSRPSTAKPSKIPTPQRKSPASKLDKSSKR; N-terminally labeled with carboxyfluorescein) | Buey et al., 2012 | |
| MACF1-p2 peptide (KPSKIPTLQRKSW) | This study | |
| Deposited Data | | |
| EB1c-Kar9c-p1 complex structure | This study | PDB: 5N74 |
| Software and Algorithms | | |
| XDS | Kabsch, 2010 | http://xds.mpimf-heidelberg.mpg.de |
| PHASER | McCoy et al., 2007 | www.ccp4.ac.uk |
| COOT | Emsley and Cowtan, 2004 | https://www2.mrc-lmb.cam.ac.uk/personal/pemsley/coot/ |
| REFMAC | Murshudov et al., 1997 | www.ccp4.ac.uk |
| PROCHECK | Laskowski et al., 1993 | www.ccp4.ac.uk |
| PYMOL | Schrödinger, LLC | www.Schrodinger.com |
| Sigmaplot, v13.0 | Systat Software Inc | www.sigmaplot.co.uk |
| Origin 2016, b9.3.2.303 | OriginLab Corporation | www.OriginLab.com |

### CONTACT FOR REAGENT AND RESOURCE SHARING

Further information and requests for resources and reagents should be directed to and will be fulfilled by the Lead Contact, Michel Steinmetz (michel.steinmetz@psi.ch)

## METHOD DETAILS

### Protein and Peptide Preparation

The N-terminally hexa-histidine tagged *S. cerevisiae* full length Bim1 (UniProtKB ID P40013), Bim1c (residues 183-344), Bim1cΔtail (residues 183-274), human EB1 (UniProtKB ID Q15691) and EB1-YE/AA constructs were cloned into the *E. coli* expression vector pSTCm-1 (Olieric et al., 2010); the N-terminally hexa-histidine tagged EB1cΔtail-Kar9c-p1 chimera (residues 191-248 of human EB1 and residues 615-633 of *S. cerevisiae* Kar9; UniProtKB ID P32526) was cloned into the pET15b bacterial expression vector (Invitrogen). Sequence verified plasmids were transformed into BL21(DE3) *E. coli* cells for protein expression. To produce the proteins, liquid cultures were shaken in LB medium containing the appropriate antibiotic to an $OD_{600}$ of 0.6. Cells were induced by the addition of 0.75 mM isopropyl-β-D-thiogalactoside (IPTG) and further incubated overnight at 20 °C.

Affinity purification of His-tagged proteins was carried out by immobilized metal affinity chromatography on $Ni^{2+}$-Sepharose columns (Amersham) at 4°C according to the manufacturer's instructions. The hexa-histidine tags were enzymatically cleaved off by thrombin treatment. For this, proteins were incubated and dialyzed at 4°C with 2 units/milligrams of thrombin in cleavage buffer (20 mM Tris-HCl, pH 8.4, supplemented with 150 mM NaCl and 2.5 mM $CaCl_2$). The tag-less protein samples were further processed on a Superdex-75 size exclusion chromatography column (Amersham) pre-equilibrated in 25 mM Tris-HCl, pH 7.5, supplemented with 150 mM NaCl. The purity of recombinant proteins was confirmed by Coomassie-stained 12% SDS-PAGE, and the identities of the proteins were assessed by mass spectral analyses. Exact concentrations of protein solutions were determined by tyrosine and tryptophan absorbance at 276 nm.

Bacterially expressed mCherryEB3, mCherryEB3Δtail, Mal3, Trx-Kar9-Site2 and Trx-Kar9-Site3 were prepared as described previously (Manatschal et al., 2016; Montenegro Gouveia et al., 2010). The Kar9c-p1 (TRRRTRLRPPTPLSQLLSP), FC-MACF1-p1 (HRPTPRAGSRPSTAKPSKIPTPQRKSPASKLDKSSKR; N-terminally labeled with carboxyfluorescein) and MACF1-p2 (KPSKIPTLQRKSW) peptides used for biophysical measurements were made by automatic solid-phase peptide synthesis on Tentagel-SRam resin (Rapp Polymere, Germany) using the Fmoc chemistry. The peptides were HPLC purified and the identity of the peptides was validated by mass spectral analyses.

### Isothermal Titration Calorimetry (ITC)

ITC experiments were performed at 25°C as described previously (Bjelic et al., 2012). Briefly, the sample cell and syringe were filled with 100 μM Bim1 or EB1 proteins (monomer equivalents) and 500 μM of Kar9c-p1 or MACF1-p2 peptide solutions, respectively. Both, the proteins and the peptides were equilibrated in the same buffer (25 mM sodium phosphate, pH 7.5, supplemented with 150 mM NaCl), filtered and degassed before the experiment. The peptides were injected in 2.5 μl aliquots into the protein solution using a MicroCal $iTC_{200}$ microcalorimeter (Microcal Inc.). Control experiments were performed by injecting peptide solutions into the buffer. The binding isotherms were fitted by a nonlinear least-squares minimization method using the Origin v8.0 software package (Microcal Inc.).

### Fluorescence Polarization Spectroscopy

Fluorescence polarization competition experiments at room temperature were performed as described previously (Buey et al., 2012). Briefly, 0.1 μM of the FC-MACF1-p1 peptide were pre-incubated with 10 μM full length Bim1 (total volume of 1 ml). 500 μM Trx-Kar9-Site2 or Trx-Kar9-Site3 protein solutions (Manatschal et al., 2016) supplemented with 0.1 μM FC-MACF1-p1 were subsequently added stepwise to the reaction mixture. The change in fluorescence polarization was monitored at 25°C on a Varian Eclipse fluorimeter equipped with motorized polarizers and thermostated, magnetically stirred cuvette holders. The fluorescence intensities were measured at λex = 485 nm at λem = 530 nm. The G-value of the instrument was determined as 1.4961.

### X-Ray Crystallography

The EB1cΔtail-Kar9c-p1 fusion (1 mM) was crystallized using the sitting drop vapor diffusion method at 20°C by mixing equal volumes of the protein and reservoir solution. Crystals were grown with a reservoir solution containing 100 mM PCTP, pH 4, supplemented with 25% PEG 1500. Single wavelength diffraction data were collected at 100 K to 2.3 Å resolution at beamline X06DA of the Swiss Light Source (Villigen PSI, Switzerland). The crystals belonged to space group $P2_1$ and contained eight EB1cΔtail-Kar9c-p1 fusion molecules in their asymmetric unit.

Diffraction data were indexed, integrated and scaled using the XDS program (Kabsch, 2010). The EB1cΔtail-Kar9c-p1 structure was solved by molecular replacement using PHASER (McCoy et al., 2007) with the structure of EB1c (PDB ID 3GJO) as a search model. Initial rigid body refinement was carried out followed by iterative cycles of model building and restrained refinement using the programs COOT (Emsley and Cowtan, 2004) and REFMAC5 (Murshudov et al., 1997) of the CCP4 suite (Collaborative Computational Project, Number 4, 1994) to improve the phases. Inspection of the resulting $F_O$–$F_C$ and $2F_O$–$F_C$ maps of the EB1cΔtail-Kar9c-p1 structure displayed density for the bound Kar9 moiety of the chimeric construct. The peptide density was further improved by eight fold density averaging around peptide. Refinement was done until convergence and TLS (Translation, Libration and Screw) restraints were included for the final cycles of the refinement. The domain definitions were determined using the TLS Motion Determination server (Painter and Merritt, 2006). The geometry of the final refined models was validated with PROCHECK (Laskowski et al., 1993).

Figures were prepared using the program PyMOL (The PyMOL Molecular Graphics System, version 1.8.2.3; Schrödinger, LLC). The details of the data collection and refinement statistics are given in Table 1.

## Microtubule Tip Tracking Reconstitution Assay

### *Mal3-Kar9c Experiments*

Reconstitution assay was performed as previously described (Manatschal et al., 2016). Briefly, GMPCPP stabilized microtubule seeds (15% Rhodamine labelled, 10% biotinylated) were adhered to base-washed and PEG-passivated coverslips via netravidin-steptavidin immobilization. Microtubule growth was initiated by the addition of 10 μM tubulin (2% Rhodamine labelled) in assay buffer (80 mM PIPES-KOH, pH 6.8, supplemented with 85 mM KCl, 4 mM $MgCl_2$, 1 mM EGTA, and 150 mM KOAc) containing an oxygen scavenger system (0.02 mg/ml catalase, 1.5 mg/ml glucose oxidase and 0.4 mg/ml glucose). Experiments with GFP-Kar9c were performed in the absence of free Rhodamine-labelled tubulin. Concentrations of proteins were 150 nM GFP-Kar9c together with 250 nM Mal3. All experiments were carried out at 37 °C. Images were recorded on an Olympus IX81 inverted microscope equipped with a total internal reflection fluorescence (TIRF) system and controlled by the Olympus Cell$^R$ software using an Olympus UAPON 100x TIRF objective (NA 1.49). Time-lapse images were acquired every 3 sec over the duration of 6 min using a CCD camera. Image analysis was performed using ImageJ and kymographs were generated using the Kymograph plugin written by Rietdorf and Seitz (http://www.embl.de/eamnet/html/body_kymograph.html).

### *EB3-Kar9c Experiments*

Reconstitution assay was performed as previously described (Doodhi et al., 2016). The reaction mixtures in MRB80 buffer contained tubulin (15 μM), Rhodamine-tubulin (0.5 μM) when indicated, methyl cellulose (0.1%), KCl (50 mM), k-casein (0.5 mg/ml), GTP (1 mM), oxygen scavenging system (20 mM glucose, 200 μg/ml catalase, 400 μg/ml glucose-oxidase, 4 mM DTT), mCherry-EB3 or mCherry-EB3Δtail (20 nM each) and Kar9c-GFP (0.64 μM). Movies were acquired in TIRF mode using Nikon Eclipse Ti-E (Nikon) microscope supplemented with the perfect focus system (PFS) (Nikon), equipped with Nikon CFI Apo TIRF 100x 1.49 N.A. oil objective (Nikon). Photometrics Evolve 512 EMCCD camera (Roper Scientific) with triple-band TIRF polychroic ZT405/488/561rpc (Chroma) and triple-band laser emission filter ZET405/488/561m (Chroma), mounted in the metal cube (Chroma, 91032) together with Optosplit III beamsplitter (Cairn Research Ltd, UK) supplemented with double emission filter cube configured with ET525/50m, ET630/75m and T585LPXR (Chroma) was used to acquire the movies in stream acquisition mode (exposure time 500 ms). Kymographs were generated in ImageJ using KymoResliceWide plugin.

## Synthetic Peptide Arrays on Cellulose Membranes (SPOT)

Cellulose membrane-bound peptide arrays were prepared according to standard SPOT synthesis protocols using a SPOT synthesizer as described in detail (Wenschuh et al., 2000; Frank, 2002; Volkmer, 2009). The synthesis was performed on Whatman-50 cellulose membranes (Whatman) using an automatic SPOT-synthesizer (INTAVIS AG). The peptides were synthesized on amino-functionalized cellulose membranes of the ester type prepared by modifying a cellulose paper with Fmoc-β-alanine as the first spacer residue. In the second coupling step, the anchor position Fmoc-β-alanine-OPfp in dimethylsulfoxide (DMSO) was used. Residual amino functions between the spots were capped by acetylation. The Fmoc group was cleaved using 20% piperidine in dimethylformamide (DMF). The cellulose-bound peptide arrays were assembled on these membranes by using 0.3 M solutions of Fmoc-amino acid-OPfp in NMP. Side-chain protection of the used Fmoc-amino acids was as follows: Glu, Asp (OtBu); Ser, Thr, Tyr (tBu); His, Lys, Trp (Boc); Asn, Gln, Cys (Trt); Arg (Pbf).

After the last coupling step, the acid-labile protection groups of the amino acid side chains were cleaved using 90% trifluoro-acetic acid (TFA) for 30 min and 60% TFA for 3h. Membrane-bound Kar9 peptide variants were washed with DMF, ethanol, and three times with TBS buffer (13.7 mM NaCl, 0.27 mM KCl, 5 mM Tris (tris(hydroxymethyl)amino-methane, pH 8.0) for 10 min each. Membranes were incubated for 3 h with blocking buffer (for 50 mL blocking buffer: 5 mL blocking buffer (Sigma–Aldrich), 2.5 g sucrose, 5 mL 10 × TBS buffer (137 mM NaCl, 2.7 mM KCl, 50 mM Tris, pH 8.0), filled up to 50 mL with water. Arrays were incubated with a solution of His-tagged full length Bim1 at a concentration of 10 μg/ml in blocking buffer at room temperature overnight.

After three times of washing with TBS buffer (10 min each) the arrays were incubated with a solution of a mouse anti polyhistidine IgG antibody (Sigma H-1029) in blocking buffer (dilution 1:10,000) for 3 h at room temperature and then washed three times with TBS. Afterwards, the arrays were treated with a solution of a horseradish-peroxidase conjugated anti-mouse IgG antibody (Sigma A-5906) in blocking buffer (dilution 1:1000) at room temperature for 1.5 h followed by three times washing with TBS (10 min each). Binding was visualized by using a chemiluminescent substrate (Uptilight HRP, Uptima) and a Lumi-Imager (Roche Diagnostics).

## Constructs, Cell Culture and Transfection

The GFP fusions of peptide fragments used in the tip tracking experiments (see Figure 2) were generated using a PCR- and recombination-based cloning strategy, where PCR fragments with homologous flanking sites were integrated into a pEGFP-C2 vector (Clontech). The dimeric versions of the peptide fragments were obtained by introducing the leucine-zipper domain of GCN4 (O'Shea et al., 1991) at the N terminus of the respective constructs using a PCR- and homologous recombination-based cloning strategy. COS-7 cells were cultured in medium that consisted of 45% DMEM, 45% Ham's F10 and 10% fetal calf serum supplemented with penicillin and streptomycin. The cells were routinely checked for mycoplasma contamination using the LT07-518 Mycoalert assay (Lonza). FuGENE 6 (Promega) was used to transfect COS-7 cells with plasmids for live cell imaging. Cells were transfected 17-21 hrs before imaging.

### Image Acquisition

Live-cell fluorescence TIRF imaging was performed on inverted research microscope Nikon Eclipse Ti-E (Nikon) with the perfect focus system (Nikon), equipped with Nikon Apo TIRF 100x N.A. 1.49 oil objective (Nikon) and iLas$^2$ system (Dual Laser illuminator for azimuthal spinning TIRF (or Hilo) illumination and Simultaneous Targeted Laser Action) from Roper Scientific (Evry, FRANCE). System was also equipped with ASI motorized stage MS-2000-XY (ASI), Photometrics Evolve Delta 512 EMCCD camera (Photometrics) and controlled by the MetaMorph 7.8 software (Molecular Devices). Stradus 488 nm (150 mW, Vortran) and OBIS 561 nm (100 mW, Coherent) lasers were used as light sources. For simultaneous imaging of green and red fluorescence, we used Optosplit III (Cairn Research, UK) equipped with the filters from ET-GFP (49002), ET-mCherry (49008) and ET-GFPmCherry (59022) filter sets (Chroma). To keep the cells at 37 °C, a stage top incubator model INUBG2E-ZILCS (Tokai Hit) was used. Images were projected onto the CCD chip at a magnification of 0.065 μm/pixel. Cells were plated on round 25 mm coverslips, which were mounted in Attofluor Cell Chamber (Thermofisher) and maintained at 37 °C and 5% CO2. Cells were imaged at 2 frames per second with 500 ms exposure for 50 s in total. Images were analyzed using MetaMorph and ImageJ software packages and prepared for publication using Adobe Photoshop.

## DATA AND SOFTWARE AVAILABILITY

Atomic coordinates and structure factors for the EB1c-Kar9c-p1 complex structure has been deposited in the RCSB Protein Data Bank (PDB) under accession number 5N74.